Water Resources Research

RESEARCH ARTICLE
10.1029/2019WR026656

Key Points:
- An efficient engineering-based method is proposed to generate initial solutions that account for both pipe diameters and slopes
- The minimization of variability of peak depths across pipes is effective to handle future uncertainties
- The proposed method is significantly more efficient and practically meaningful than traditional approaches for UDS design problems

Supporting Information:
- Supporting Information S1
- Data Set S1
- Data Set S2
- Figure S1
- Figure S2

Correspondence to:
F. Zheng,
feifeizheng@zju.edu.cn

Citation:
Lin, R., Zheng, F., Savic, D., Zhang, Q., & Fang, X. (2020). Improving the effectiveness of multiobjective optimization design of urban drainage systems. *Water Resources Research*, *56*, e2019WR026656. https://doi.org/10.1029/2019WR026656

Received 1 NOV 2019
Accepted 29 APR 2020
Accepted article online 8 MAY 2020

Improving the Effectiveness of Multiobjective Optimization Design of Urban Drainage Systems

Ruozhou Lin[1], Feifei Zheng[1], Dragan Savic[2,3], Qingzhou Zhang[1], and Xiangen Fang[1]

[1]College of Civil Engineering and Architecture, Zhejiang University, Hangzhou, China, [2]KWR Water Research Institute, Nieuwegein, The Netherlands, [3]Centre for Water Systems, University of Exeter, Exeter, UK

Abstract Capacity of urban drainage systems (UDSs) can substantially influence flooding properties of urban catchments. This motivates many studies to optimally design UDSs often using multiobjective evolutionary algorithms (MOEAs) as they can explore trade-offs between conflicting objectives (e.g., cost vs. system reliability). However, MOEA-based approaches are typically computationally demanding and their solutions are often practically unacceptable as engineering domain knowledge is often not explicitly considered. To address these two issues, this paper proposes an efficient optimization framework for UDS design, where an engineering-based design method (EBDM) is developed to generate approximate solutions to initialize the MOEA's search, thereby greatly enhancing the optimization efficiency. To improve the solution practicality, two ideas have been implemented in the proposed optimization method (PM): (i) the variability of peak depths across pipes is minimized and (ii) a constraint is introduced to ensure that sizes of pipes in the downstream direction are no smaller than their corresponding upstream diameters. Two real-world UDSs of different size are used to demonstrate the effectiveness of the PM. Results show that (i) the proposed EBDM is effective in producing initial solutions that are very close to the final solutions identified by the optimization methods, (ii) the minimization of the variability of peak depths in pipes is practically meaningful as it can facilitate to identify solutions with great ability in handling future uncertainties (e.g., rainfall variability), and (iii) the PM significantly improves optimization efficiency and solution practicality compared to the traditional optimization approach, with benefits being more prominent for larger UDSs.

1. Introduction

Urban floods are one of the most serious natural disasters around the world, often resulting in significant damage to the economy and environment and even loss of lives (Westra et al., 2014). Occurrences of urban floods can be attributed to a number of different factors, such as intensified rainfall in a changing climate (Berg et al., 2013; Zheng et al., 2015), increased surface runoff due to urbanization (Gulbaz & Kazezyilmaz-Alhan, 2017; Hammond et al., 2013), and inappropriate design of urban drainage systems (UDSs) (Lowe, 2010; Schmitt et al., 2004). The performance of a UDS is critical as it can significantly affect the severity and spatial distribution of flooding, especially for flash floods that often occur in many countries including China (Li et al., 2015).

Traditionally, the design of a UDS is based on an intensity-duration-frequency (IDF) curve that has often been derived from local rainfall properties and catchment characteristics (e.g., size and slope) (Arnbjerg-Nielsen, 2012). More specifically, within a typical UDS design process, a critical duration (e.g., 3 hr) is often identified for the catchment being considered, representing the rainfall duration that has the most significant influence on the flooding of this catchment (Westra et al., 2014). The selection of the critical duration is followed by an estimate of the rainfall event for a given return period (e.g., 20-year return period, which is often derived using statistical methods) with an assumed temporal distribution (e.g., Chicago curve, Pan et al., 2017). Finally, the sizes of the UDS elements can be identified with the aid of hydraulic calculations (e.g., Manning formula; Yen, 1992) based on the given rainfall properties. While this traditional method has a high practical value due to its simplicity, the resultant UDS solutions are often either underdesigned (i.e., the resultant solutions are unable to convey the runoffs produced by the design precipitation events), resulting in increased flood risk, or overdesigned, leading to unnecessarily high capital investment. This

is, at least partly, because these traditional IDF-based methods often assumed a temporal distribution for the designed rainfall extremes (e.g., Chicago curve), which can be significantly different from the true rainfall processes especially in a changing climate (Jato-Espino et al., 2016).

In recent years, observed temporal distributions of rainfall events (i.e., observed hyetographs) are increasingly used for UDS designs at locations where a sufficiently long period of precipitation data is available (Dawadi & Ahmad, 2012). This approach is often referred to as the event-based method, in which observed rainfall events are selected as inputs for a hydrologic-hydraulic simulation model to identify suitable UDS configurations (Zheng et al., 2014). Compared to the traditional IDF-based method, a key advantage of the event-based approach is its ability to explicitly account for observed rainfall processes. As a result, this event-based approach is more likely to produce UDS design solutions that are sufficient to accommodate the runoffs associated with the precipitation events with a specific return period (Fu & Butler, 2014).

Within the event-based method, optimization techniques are often employed to identify UDS solutions with the best possible performance and at the lowest cost. This is important as UDS designs are often associated with potentially large investment (Navin et al., 2019; Zhou, 2014). Typically, such optimization runs are performed with the aid of evolutionary algorithms (EAs) combined with hydrologic-hydraulic simulation models that can explicitly consider the temporal distribution of rainfall extremes (Barreto et al., 2010; Zheng et al., 2014). Starting from single objective optimizations, which solely consider minimization of the UDS design cost (Ahmadi et al., 2018; Lowe, 2010), in recent years there has been a significant move toward the multiobjective optimization domain (Houng & Pathirana, 2013). A key advantage of the multiobjective framework is its capacity to explore trade-offs between conflicting objectives. For example, cost and system reliability can be considered (Farmani et al., 2005; Maier et al., 2014), where the latter can be used to measure the potential ability of UDS design solutions to handle future uncertainties associated with rainfall (Wasko & Sharma, 2015) and catchment runoffs (Hoss et al., 2016).

In recognizing the benefit of the event-based multiobjective design optimization method as stated above, some studies used this approach to identify the optimal UDS designs. For example, Barreto et al. (2010) used a multiobjective evolutionary algorithm (MOEA) to optimize the design of UDSs, in which the minimization of investments and the minimization of flood damages were considered as two objectives. Subsequently, Vojinovic et al. (2014) described a multiobjective design approach, where uncertainties due to climate change, urbanization, population growth, and aging of pipes were incorporated into the design and rehabilitation of UDSs. More recently, Duan, Li, and Tao (2016) and Duan, Li, and Yan (2016) employed an MOEA to design detention tanks within UDSs, in which the Monte Carlo simulation was adopted to consider uncertainties associated with rainfall, land use variations and other factors. In addition, Yu et al. (2017) proposed a stochastic model to analyze the trade-off between UDS cost and flood damages, while Wang et al. (2018) compared the performance of a few MOEA optimization methods applied to the UDS design problems.

While the MOEA-based methods have been successfully applied to identify optimal design solutions for UDSs, their applications in practice are not without difficulties. One critical issue is the low convergence rate, which affects computational efficiency associated with the MOEA-based optimization methods (Broad et al., 2004; Fu et al., 2009; Wang et al., 2018). This is because fitness evaluation and the search mechanisms of the MOEAs rely on physically based UDS simulation models, which can be computationally demanding (Maier et al., 2014). For example, a preliminary test has been carried out in the present study where a UDS with 53 pipes was optimized by a benchmark MOEA algorithm Borg (Hadka & Reed, 2013) combined with a freely available simulation software Stormwater Management Model (SWMM, Rossman, 2010). Simulation results showed that this optimization needed approximately 360 hr (15 days) on a 2.9-GHz Dell PC (Inter R) if 1,000,000 evaluations were allowed. Such a large evaluation number was typically required for MOEAs in practical applications (Wang et al., 2015). This computational overhead can significantly exceed the timeframe that is typically available for the UDS design, which often ranges from a few hours to couple of days (Wang et al., 2015). Although some techniques have been developed to improve the computational efficiency regarding the MOEA optimization for UDS designs, such as metamodels (Fu et al., 2009) and the GA-HP model (Hassan et al., 2018), their performance still remain poor, especially when dealing with large real-word UDSs (Maier et al., 2014).

In addition to low efficiency, another issue with the MOEA-based approaches is that the identified UDS design solutions are often impractical for implementations. This issue has been often ignored within the

multiobjective optimization framework (Walski, 2001). For instance, the majority of previous MOEA-based optimization methods did not explicitly consider the engineering criterion of the UDS design that the size of a pipe should be no smaller than its upstream pipes (Ngamalieu-Nengoue et al., 2019; Vojinovic et al., 2014; Yazdi, 2018). In addition, many previous approaches only used simple statistics, for example, the mean or sum of the flood volumes or peak flows in the pipes, as the objective to represent the system reliability (Liu et al., 2018; Mohammadiun et al., 2018). However, these simple statistics can be practically less meaningful as they cannot indicate the spatial distribution of the flood volumes/peak flows within the entire UDS. This can result in potentially high flood risk for some regions with large values of flood volumes/pipe peak flows.

To address the two issues as stated above, this paper proposes a multiobjective optimization framework, aimed to significantly improve the effectiveness of the UDSs design solutions. In this approach, the optimization of the UDS design problem is formulated using three objectives, primarily focusing on the cost and the system reliability in dealing with future uncertainties. Meanwhile, within this optimization framework, the engineering criterion that the size of each pipe should be no smaller than its upstream pipes is explicitly considered as the constraint. Based on the defined objective functions and constraints, an engineering-based design method (EBDM) is proposed to generate approximate optimal solutions to initiate the MOEA search, thereby greatly enhancing the optimization efficiency for identifying optimal solutions.

2. Methodology

The overall methodology of the PM is presented in Figure 1. As shown in this figure, first, a three-objective optimization model is formulated, followed by the description of the three objectives and the constraints involved. Second, the proposed EBDM is introduced to generate approximate solutions for the three-objective optimization model, in which the rational approach is employed as the hydraulic fundamentals for the proposed sampling method. Finally, these approximate solutions are used to provide initial solutions to initialize an MOEA algorithm. Consequently, the final Pareto fronts (set of optimal solutions) can be identified with significantly improved effectiveness, where both the optimization efficiency and solution practicality are enhanced.

2.1. A Multiobjective Optimization Framework for the UDS Design Problems

In the PM, the decision variables considered are the sizes of the pipes as well as their slopes for the given UDS with a total of n pipes; that is, $\mathbf{V} = [D_1, D_2, ..., D_n; S_1, S_2, ..., S_n]^T$, where D_i and S_i are the diameter and slope of pipe $i = 1, 2, ..., n$, respectively. The three objectives considered are the minimization of the cost (Equation 1), the minimization of the average peak relative water depths (APRD) in pipes and the standard deviation of the relative peak water depths (SDRPD) in pipes for a given precipitation return period (Equations 2 and 3). The detailed formulation is given as follows:

Minimize the cost:

$$C_T = \sum_{i=1}^{n} \frac{1.32}{2000}\left(9579.31 {D_i}^{0.5737} L_i + 1163.77 {Ve_i}^{1.31}\right) \tag{1}$$

$$Ve_i = (UE_i + DE_i + 2D_i + 0.3)(0.5 + D_i) L_i \cos(\cot(S_i))$$

Minimize the APRD:

$$\overline{e} = \frac{1}{n} \sum_{i=1}^{n} \frac{h_i}{Dm_i} \tag{2}$$

Minimize the SDRPD:

$$\sigma = \sqrt{\frac{1}{n} \sum_{i=1}^{n} \left(\frac{h_i}{D_i} - \overline{e}\right)^2} \tag{3}$$

No flooding at each manhole:

$$V_j = 0 \tag{4}$$

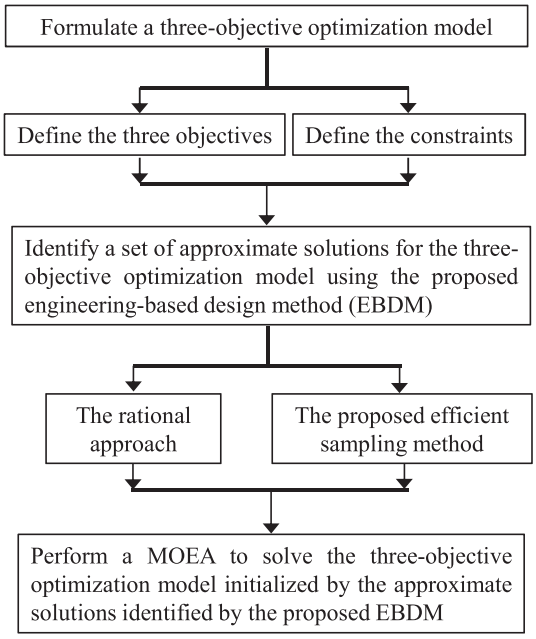

Figure 1. The main steps of the proposed optimization method.

Relative peak water depth of the pipe:

$$e_{\min} \le \frac{h_i}{D_i} \le e_{\max} \tag{5}$$

Velocity range at pipe peak flows:

$$v_{min} \le v_i \le v_{\max} \tag{6}$$

Minimum allowable slope of the pipe:

$$S_{\min} \le S_i \tag{7}$$

The size of the pipe should be no smaller than the maximum value of its corresponding upstream pipes (the practicality constraint):

$$D_i \ge Max\{\Omega(D_i)\} \tag{8}$$

Diameter choices:

$$D_i \in Z \tag{9}$$

Minimum cover depths at both ends of the pipe:

$$E_{\min} \le UE_i,\ E_{\min} \le DE_i \tag{10}$$

where C_T is the total cost of the pipe material and the constructions (U.S. dollars); D_i is the diameter of pipe i (mm); L_i is the length of pipe i (m); Ve_i is the excavation volume required for placing the pipe (m^3), UE_i (m) and DE_i (m) are the pipe cover depth of its upstream end and downstream end respectively. It is noted that Equation 1 was taken from Navarro (2009), which was derived from engineering experience. The cos and cot are cosine and cotangent in trigonometric functions, respectively.

In Equation 2, h_i is the peak water depth in pipe i for a given precipitation event, and $\frac{h_i}{Dm_i}$ is the peak relative water depth, where Dm_i is the maximum allowable water depth for the drainage pipes. Please note that Dm_i equals to D_i in the current study as all drainage pipes considered are circular conducts. The metric of APRD ranges from 0 to 1, with a smaller value representing overall lower water depths in the pipes and hence these pipes can have larger volume to accommodate the unexpected storm water due to uncertainties (e.g., rainfall uncertainty). The standard deviation of relative peak water depths (SDRPD) in Equation 3 is used to measure the variation of the relative peak water depth across the UDS. It can be easily deduced that the first two objectives considered (Equations 1 and 2) are inherently conflicting, as cost saving often leads to small pipe diameters and hence high APRD values for a given rainfall return period. In addition, the minimization of the SDRPD (Equation 3) can lead to an overall equalization of relative peak water depths in the pipes located in different regions, thereby increasing the system's overall ability to handle uncertainties such as spatial variations of precipitations (Zheng et al., 2015).

In terms of constraints that need to be considered, no overflows at the manholes of the UDS under a given rainfall return period are often used (Equation 4); that is, $V_j = 0$, where V_j is the flood volume (m^3) at manhole $j = 1, 2, ..., m$, within a UDS with m manholes. It is noted the surcharges at the manhole or in the pipes are not considered as the constraints in this study, where the hydraulics associated with the surcharges are simulated using the dynamic wave method from the SWMM package. The relative water depth in a pipe is often practically limited within a given range between the minimum ($e_{\min}$) and maximum ($e_{\max}$) values to avoid too large or too small pipe sizes, as shown in Equation 5. It is noted that Equation 5 calculates the water depth in the pipes rather than the manholes, and hence, it is different to Equation 4 that is used to avoid flooding in the manholes. In addition, Equation 5 is not applied to the case when the maximum water depth of the minimum allowable pipe diameter is still lower than $e_{\min}$, in order to generate feasible design

solutions. As indicated in Equation 6, the minimum and maximum velocities at peak flow in each pipe are often limited to avoid sediment deposition (v_{min}) and flushing (v_{max}), which are 0.75 and 10 m/s, respectively (Beijing General Municipal Engineering Design & Research Institute, 2017). In addition, the slope of each pipe cannot be smaller than the given minimum value (Equation 7).

The practicality constraint in Equation 8 ensures that the diameter of pipe D_i should be no smaller than the maximum value of all its intermediately upstream pipes ($\Omega(D_i)$) based on the engineering domain knowledge and engineering rules. Equation 9 indicates that diameters for pipes can only be selected from a discrete set of Z, which represents the commercially available sizes, and the cover depths of the ends of the pipes should be large enough to avoid damages induced by traffic loads on the ground (i.e., $UE_i > E_{min}$, $DE_i > E_{min}$ in Equation 10). It should be noted that the final optimal solutions have to strictly satisfy all constraints mentioned above (Equations 4–10). The proposed methodology in the current paper focuses on the UDS design with circular conducts, which is the typical case in urban areas. However, this methodology can be extended to handle the design cases where noncircular conducts are involved, and for such cases, the maximum allowable water depth (Dm_i in Equation 2) and the available sizes of the noncircular conducts need to be slightly modified.

2.2. The Proposed EBDM

2.2.1. The Rational Approach

Traditionally, the rational approach (Mccuen, 2004) has been widely used for UDS designs in many countries such as China (Code for Design of Outdoor Wastewater Engineering, CDOWE, 2014). Within this method, the flows of pipe i, Q_i (L/s), are determined using

$$Q_i = \phi_i q F_i \tag{11}$$

$$q = \frac{a(1 + c\lg P)}{(t_i^1 + t_i^2 + b)^d} \tag{12}$$

where ϕ_i is the runoff coefficient of the subcatchment (often specified by users) associated with pipe i with an area of F_i (m^2); q (L/s/m^2) is the rainfall intensity over the entire catchment, which is determined in a semiempirical manner (Equation 12). Parameters a, b, c, and d are identified based on the fit of rainfall observations; P is the rainfall return period; t_i^1 is the concentration time of the subcatchment associated with pipe i and t_i^2 is total traveling time of the runoffs from the upstream pipes of pipe i (t_i^2=0 if pipe i is the first upstream pipe).

For the given diameter, slope, and design water depth, the hydraulic capacity Q_{ci} of pipe i can be computed using Manning equation (Gupta, 2016).

$$Q_{ci} = \frac{1}{nc_i} A_i (R_i)^{2/3} (S_i)^{1/2} \tag{13}$$

where nc_i is the manning coefficient of pipe i (specified by users); A_i is the cross sectional area of pipe i; R_i is the hydraulic radius with $R_i = A_i/W_i$ (W_i is the wetted perimeter), and S_i is the slope of the pipe. For a given peak relative water depth $\frac{h_i}{D_i}$ (i.e., θ is known), the slope and diameter of the circular pipe i under a given $\frac{h_i}{D_i}$ can be derived as

$$D_i = \left\{ \frac{20.16 \times nc_i Q_{ci} \theta_i^{2/3}}{(\theta_i - \sin\theta_i)^{5/3} S_i^{1/2}} \right\}^{3/8} \tag{14}$$

where nc_i is a known value, Q_{ci} should be no smaller than Q_i determined using Equation 11. As indicated by Equation 14, the diameter D_i and slope of pipe S_i are strongly dependent, which can be determined through a trial-and-error method (Butler et al., 2018). However, within practical applications, it is difficult, if not impossible, to ensure all the constraints (Equations 4–9) are satisfied using the trial-and-error method applied to Equation 14, especially for large real-world UDSs. To address this problem, the

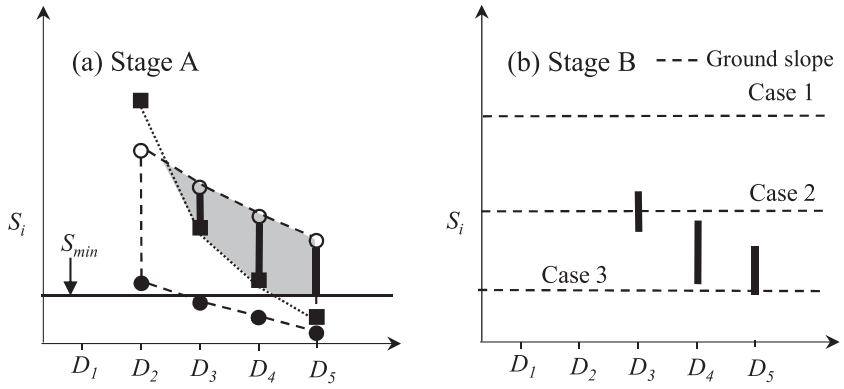

Figure 2. Illustration of the proposed efficient sampling method. In (a), the empty and filled circle points as well as the dashed lines are determined in Step A4, squares connected by dotted lines are determined in Step A5, the gray shaded region represents the feasible region, and vertical solid lines represents the diameters and slopes for pipe i with all constraints satisfied (the same in (b)).

present paper proposes an efficient sampling method to identify approximate values of D and S for each pipe, which is accordingly used to initialize the MOEA.

2.2.2. The Proposed Efficient Sampling Method

Prior to the implementation of the proposed efficient sampling method, all pipes of the UDS have to be indexed, with lower index values representing pipes at more upstream locations (e.g., the index 1 indicates the most upstream pipe). Such indexing can be achieved based on the given topology of the UDS, and more specifically the upstream-downstream relationships of different pipes. For a known $\frac{h_i}{D_i}$ within the prespecified range in Equation 5 (i.e., θ is known), the proposed sampling method can be divided into two primary stages. In Stage A, the feasible region that satisfies all constraints from Equations 4–9 is determined for each pipe, followed by the identification of approximate values of D and S for this pipe in Stage B. The proposed sampling method is applied to all the pipes in a sequencing manner based on the index values (i.e., from the upstream to the downstream). The detailed steps of the proposed efficient sampling method applied to pipe i are outlined below, with Figure 2 illustrating these steps.

Stage A: Determine the feasible region for pipe i.

Step A1: Consider all the available commercially discrete diameter sizes for pipe i (satisfy Constraint 9), and in Figure 2 $[D_1, D_2, D_3, D_4, D_5]^T$ is used for illustration.

Step A2: Identify the diameter sizes that can be used for pipe i based on the engineering criterion where the size of pipe i should be no smaller than the maximum value of its corresponding upstream pipes ($\Omega(D_i)$, satisfy Constraint 8). If $i = 1$, this pipe is the most upstream pipe and hence all the commercially available diameter sizes can be used. In the exampled case in Figure 2a, it is assumed that $Max\{\Omega(D_i)\} = D_2$ and hence $[D_2, D_3, D_4, D_5]^T$ can be considered for pipe i.

Step A3: Set the minimum allowable slope $S_{\min}$ according to Equation 7 as shown by the horizontal solid line in Figure 2a.

Step A4: For each diameter size that can be potentially used for pipe i (identified by Step A2), use the following equation (derived from basic flow Equation 13) to determine its minimum (filled circle points in Figure 2a) and maximum (empty circle points in Figure 2a) allowable slopes S:

$$S_i = \frac{v_i^2 n c_i^2}{\left(0.25 D_i \frac{\theta_i - \sin\theta_i}{\theta_i}\right)^{\frac{2}{3}}} \tag{15}$$

where D_i is replaced by each of the available diameter sizes; $v_i$is replaced by the prespecified minimum or maximum allowed velocities in the constraint (Equation 6). As indicated by the dashed line in Figure 2a, a region is formed by connecting the minimum and the maximum slope values.

Step A5: To satisfy Constraint 4 where no flooding is allowed, the capacity of pipe i should be no lower than the designed flow rate Q_i. In other words, for each D_i identified by Step A2, its slope S_i should be no smaller than the slope identified by Equation 14 (Squares in Figure 2a), which can be expressed as

$$S_i \geq \left\{ \frac{20.16 \times nc_i Q_i \theta_i^{2/3}}{(\theta_i - \sin\theta_i)^{5/3} D_i^{8/3}} \right\}^{3/4} \tag{16}$$

Consequently, the feasible region for pipe i is identified (the gray shaded region in Figure 2a) as the intersection of the $S_{\min}$ (the horizontal solid line) in Step A3, the region formed in Step A4, and dotted lines used to connect squares as determined in Step A5. Given that only discrete diameter sizes can be used, the diameters, as well as associated slopes for pipe i with all constraints satisfied (Equations 4–9), are represented by the vertical black solid lines within the feasible region, which are shown in Figure 2b for clear illustration.

Stage B: Identify reasonable D_i and S_i values for pipe i.

Step B1: Based on the identified feasible region for pipe i (the vertical solid lines in Figure 2b), the minimum diameter within this region is selected (D_i). This is because relatively small diameter sizes are often associated with low costs. Furthermore, by assigning a small diameter to pipe i there would be more diameter options left for its downstream pipes. For the shown example, $D_i = D_3$ is selected for pipe i.

Step B2: For the fixed diameter size of pipe i (D_i), the ground slope associated with pipe i is used to identify its appropriate slope (S_i). When the ground slope is higher than the maximum allowable slope associated with D_i (Case 1 in Figure 2b), the maximum allowable slope of D_i is used as S_i. If the value of the ground slope is between the minimum and maximum allowable slopes of D_i (Case 2), the ground slope is taken as S_i. For Case 3, when the ground slope is smaller than the minimum allowable slope of D_i, this minimum slope is used as S_i. Such a rule is based on the rationale that it is typically cost effective to ensure the slope of pipe follows its associated ground slope as close as possible, thereby reducing the cost associated with excavating volume required for placing the pipe (Navarro, 2009).

2.3. MOEA Optimization Framework and Solution Analysis Methods

In the PM, a set of different design peak relative water depths $\left(\frac{h_i}{D_i}\right)$ within the given range and with a specified resolution (e.g., 0.05) is used to identify the approximate design solutions. For each given design value of $\frac{h_i}{D_i}$, all pipes are assigned this particular value, followed by the implementation of the proposed EBDM, thereby generating a series of initially feasible and reasonable solutions. These solutions are employed to initialize the MOEA run. This allows the search process to further improve solution quality in an efficient manner with the observed precipitation considered.

The result analysis is conducted in the solution space to demonstrate the efficiency enhancement of the PM, as well as in the decision space to demonstrate the utility of the PM in improving the engineering practicality of the design solutions. As previously stated, Constraint 8 is not considered for the TOM as many previous MOEA-based optimization methods did not explicitly consider this important engineering criterion within the UDS design process (Yazdi, 2018). Therefore, a metric of practicality level (PL) is introduced to facilitate the engineering practicality analysis for the optimal solutions, which is defined as

$$I_i = \begin{cases} 1, & D_i \geq Max\{\Omega(D_i)\} \\ 0, & \text{otherwise} \end{cases} \tag{17}$$

$$PL = \frac{1}{n} \sum_{i=1}^{n} I_i \times 100\% \tag{18}$$

For a given design solution, a larger value of PL indicates that a larger proportion of pipes satisfy the engineering design criterion (Constraint 8), indicating improved engineering practicality. For example, PL = 100% and 90% indicating that all the pipes and 90% of the pipes in the solution satisfy Constraint 8, respectively.

3. Experiment Design

3.1. Case Studies

Two UDSs located in Hang Zhou, a city in China, were selected to demonstrate the effectiveness of the PM. Case Study 1 is a university campus with a drainage area of 0.081 km^2 and 19 subcatchments. This UDS contains 19 pipes with a total length of 1.3 km and ground slopes ranging from 3‰ to 10‰. The system has 19 manholes and 1 outlet. Figure 3a shows the catchment land use of Case Study 1, while Figure 3b presents the schematic of the network used for modeling. Case Study 2 has a drainage area of 0.29 km^2 consisting of 53 subcatchments with slope ranging from 4.1‰ to 11‰ and its land use types as well as a schematic of the network are shown in Figure 4. This system has 53 pipes, 53 manholes, and 1 outlet. The types of land use for Case Study 2 are outlined in Figure 4a, and Figure 4b shows the schematic of drainage system.

The SWMM was used to enable the hydraulic simulations for the two case studies, where the dynamic wave method and the Horton equation were employed to simulate the hydraulics and the infiltrations respectively. The properties of the two catchments, including pipe lengths, ground slopes and subcatchment sizes can be found in the supporting information of this paper. A 3-hr precipitation time period with a return period of 5 years ($P = 5$) was used for the two case studies to enable the design of these systems based on the requirement of the local water utility. A typical precipitation event (Figure 5) with a 5-year return period was selected from the observations and was applied to the two UDSs.

3.2. Application of the Proposed EBDM

For the two case studies considered, the minimum and maximum relative water depths were 0.4 and 1.0 respectively, that is, $e_{min} = 0.4$ and $e_{max} = 1.0$ in Equation 5 following the specification of the local water utilities. Within this range, a total of 20 discrete relative water depths (i.e., with an interval of 0.03) was used to generate the initial solutions using the proposed EBDM. It should be noted that, for each selected value of peak relative water depths, this value was applied to all pipes within each UDS to determine their diameters. According to the land use and pipe information provided by the local water utility, the Manning coefficient was selected to be $n_c = 0.013$ for all pipes within both case studies. The parameter values for the precipitation intensity equation (Equation 12) were also provided by the local water utility, with $a = 57.694$, $b = 31.546$, $c = 0.93$, and $d = 1.008$. For the two case studies, a range of different commercially available diameter options were considered, which were 300, 400, 500, 600, 700, 800, 900, 1,000, 1,200, 1,350, 1,500, 1,650, 1,800, 2,000, 2,200, and 2,400 mm.

3.3. Application of the MOEA Optimization

Borg was selected as the MOEA optimization in this study due to its efficient and effective searching capacity on water resources optimization problems (Hadka & Reed, 2013; Wang et al., 2015; Zheng et al., 2016, 2017). Borg was a hybrid MOEA, combining ε-dominance, ε-progress, randomized restart, and autoadaptive multioperator into a unified framework, with details given in Hadka and Reed (2013). To enable a comprehensive comparison, the traditional optimization method (TOM), where Borg was applied in combination with random initialization, was also applied to the two case studies. Both the TOM and the PM used the same objective functions and constraints in Equations 1–10, with only difference being that the former did not consider the engineering criteria (the constraint in Equation 8).

For each optimization method, the maximum allowable number of evaluations was set to 500,000 for both case studies. The initial population size for the two optimization methods applied to both case studies was 1,000, and this value was self-adaptively changing during the runtime as a result of the applications of Borg operators. These parameter values (i.e., the number of evaluations and the population sizes) were determined through a preliminary analysis. It is noted that the number of initial solutions offered by the proposed EBDM was limited and hence some random solutions were also generated in the PM to ensure the total number of initial solutions equaled the specified population size for each case study. For each optimization method applied to each case study, a total of 10 runs was performed with different random number seeds. It was noted that the final Pareto fronts were overall similar across different runs for the PM, but the traditional method (TOM) exhibited a moderate performance variation over different runs. A typical run of the PM was used to enable the performance comparison with the best run of the TOM, with results and discussion shown below. It is noted that the number of initial solutions generated by the proposed EBDM was 20 for each case study, which is rather small relative to the population size of 1,000 used for Borg applied to these two case

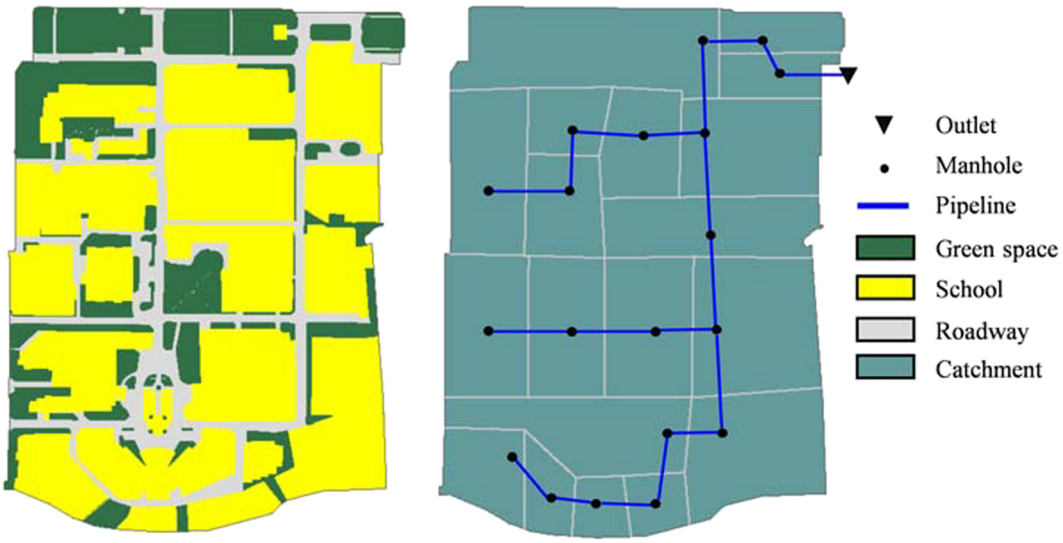

Figure 3. Case Study 1: (a) land uses and (b) the drainage system.

studies. Consequently, the inclusion of the EBDM solutions would not result in premature convergences of Borg, which was also confirmed by the observations in the simulation study.

4. Results and Discussions

4.1. Analysis of Solutions From the EBDM

Figure 6 shows the resultant design solution for Case Study 1 produced by the EBDM with the peak relative water depth of 1 (i.e., full pipe). The hydraulics of this design solution were simulated using the observed rainfall event given in Figure 5 rather than the semiempirically determined rainfall series used in EBDM,

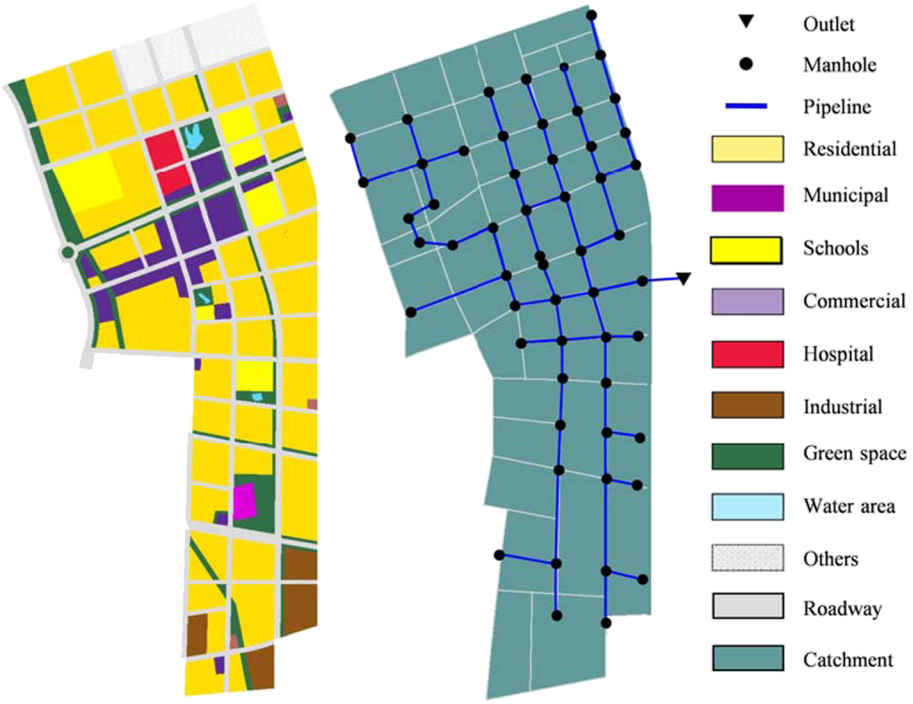

Figure 4. Case Study 2: (a) land uses and (b) the drainage system.

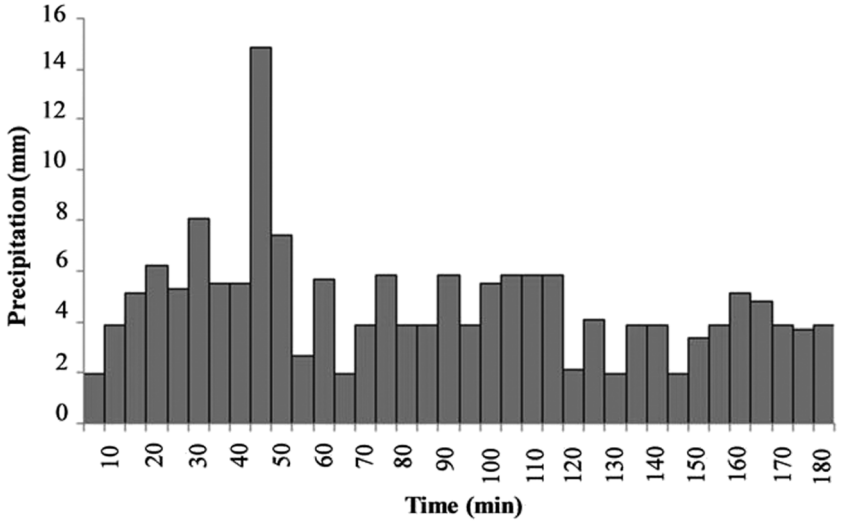

Figure 5. The observed hyetograph of a typical precipitation event for a period of three hours with a 5-year return period.

with flooded manholes representing by shaded nodes in red. It is highlighted that the design solution identified by the EBDM could have flooding nodes due to that the true rainfall process was not explicitly considered. As shown in Figure 6, while all pipes were designed with a peak relative water depth of 1, the resultant true peak relative water depths can be substantially different from this design value with the minimum value being only 0.38 for P5. This is because the assumed temporal distribution of this event (Equation 8) within the proposed EBDM method is significantly different to the truly temporal distribution given in Figure 5. Two out of 19 manholes were flooded for the design solution produced by the proposed EBDM, implying that the diameters associated with these two manholes were insufficient to accommodate the runoffs caused by the true rainfall event.

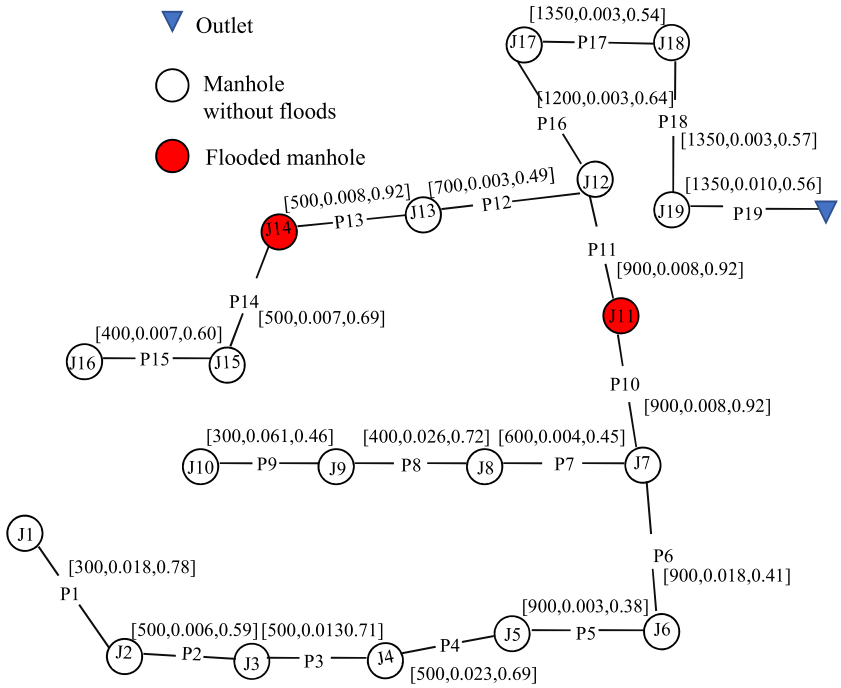

Figure 6. The simulated hydraulics for a design solution from the proposed EBDM with a relative peak water depth of 1 for Case Study 1. Square brackets show the diameter (mm), pipe slope, and the relative peak water depth of each pipe. *J* and *P* indicate nodes and pipes, respectively.

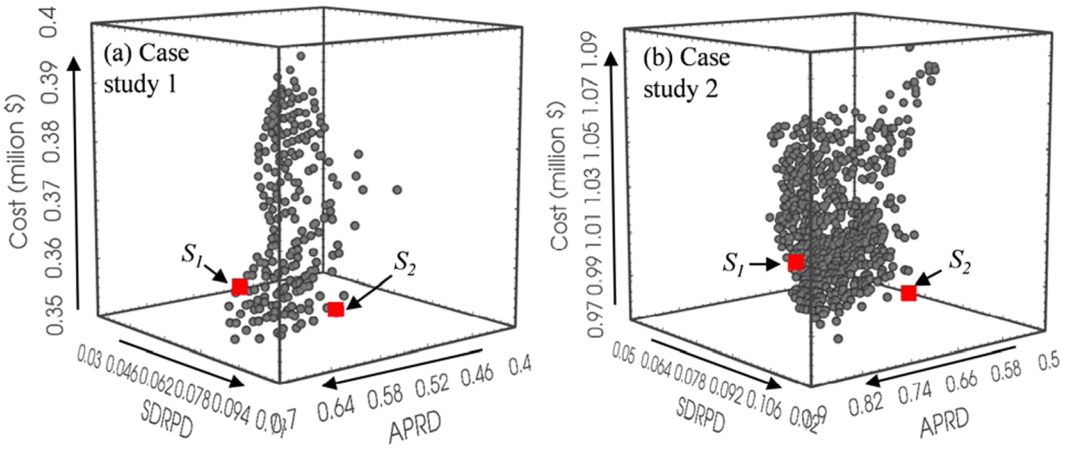

Figure 7. The final optimal fronts produced by the proposed method applied to the (a, b) two case studies.

As shown in Figure 6, while the design solution generated by the proposed EBDM violated the constraint in the solution space (i.e., no flooding) at a few nodes, it was overall reasonable as the majority of manholes within the system did not flood. More importantly, this solution satisfied all the other constraints from Equations 5–10. Similar observations can be made for other solutions produced by the EBDM applied to the two case studies. This implies that although the solutions generated by the proposed EBDM may not be directly adopted for practical applications, they can be considered as the approximate optimal solutions.

4.2. Objective Analysis of the Final Optimal Fronts

Figure 7 shows the final optimal fronts produced by the PM applied to the two case studies. It shows that, for Case Study 1, the average peak relative water depth (APRD) ranged between 0.4 and 0.7, and the cost varied between 0.35 and 0.40 million U.S. dollars. For Case Study 2, the value of APRD reached 0.9, and the cost varied between 0.97 and 1.1 million U.S. dollars. These differences between the two case studies were caused by the variation of individual catchment properties.

In terms of the standard deviation of relative peak water depths (SDRPD) in pipes, it was observed that both case studies had relatively low values of SDRPD, as shown in Figure 7. Two nondominated solutions with similar costs were selected from each of the two case studies for detailed analysis (red squares in Figure 7), with the distributions of relative peak water depths of pipes given in Figure 8. It was highlighted that the criterion for the selection of these two solutions was that they have similar costs. In this paper, the two solutions in Figure 7 were used for illustration purpose, and similar observations were made for many other solutions with similar costs. For S_1 of Case Study 1, the cost was 0.36 million dollars, APRD = 0.63, and SDRPD = 0.07, and for S_2 the cost was 0.36 million dollars, APRD = 0.61 and SDRPD = 0.10. For Case Study 2, the cost of S_1 was 0.99 million dollars, APRD = 0.75 and SDRPD = 0.08, and for S_2 the cost was 0.99 million dollars, APRD = 0.72 and SDRPD = 0.12.

As can be seen from Figure 8, for both case studies, while the solutions S_2 possessed lower APRD values than S_1, the peak relative water depths of the pipes within the former solutions were significantly more variable relative to the latter solutions. This was especially the case for Case Study 2 (S_2) as its largest relative peak water depth can get up to 1, which was significantly higher than the largest value of S_1 (about 0.85). This implies that some regions within S_2 solutions for both case studies can be more vulnerable to floods induced by future uncertainties such as spatial variation of extreme rainfalls and land use variations (Zheng et al., 2015). It was observed that S_2 of Case Study 2 possessed a relatively high density at the peak relative water depth of 1 as shown in Figure 8b. This is because this solution had some surcharged pipes and hence their peak relative water depth was 1.

To further demonstrate the necessity of the inclusion of the proposed SDRPD objective within the PM, the PM with only two objectives of the cost and APRD (referred as PMTO) was applied to the two case studies using the same computational budgets and algorithm parameterizations (e.g., initial population size) as

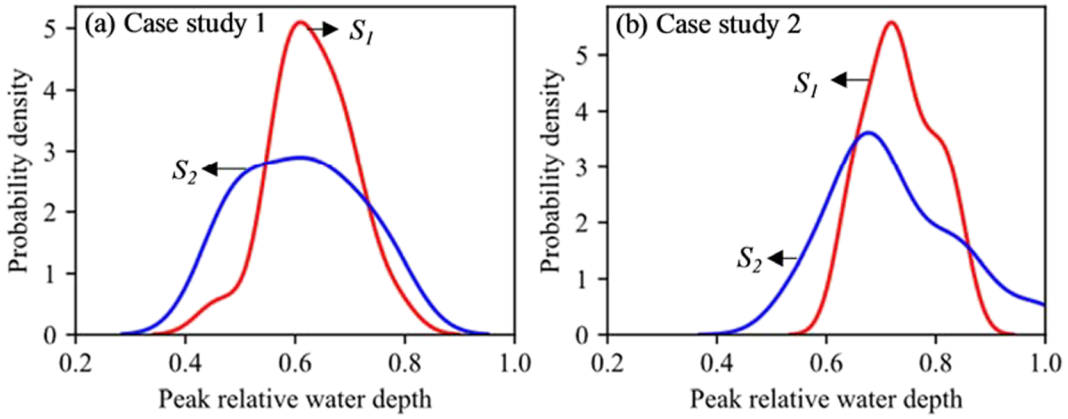

Figure 8. Density distributions of peak relative water depths of pipes for two solutions (S_1 and S_2) for each of the (a, b) two case studies.

for the PM with all the three objectives. Figure 9 shows the results in the two-dimensional space. It is seen from Figures 9a and 9c that the PMTO was able to find a similar and even better cost-APRD front than the PM with three objectives using the same computational efforts. This is because the fitness landscape defined by the three objectives can be significantly more complex than that associated with the two objectives, and hence, the PMTO is capable to identifying better fronts. When all the PMTO solutions were evaluated using the SDRPD objective (Figures 9b and 9d), it was found that these SDRPD values were overall significantly higher than those from the PM with three objectives. This implies that the inclusion of the SDRPD objective within the optimization process can identify many solutions with similar costs, slightly higher

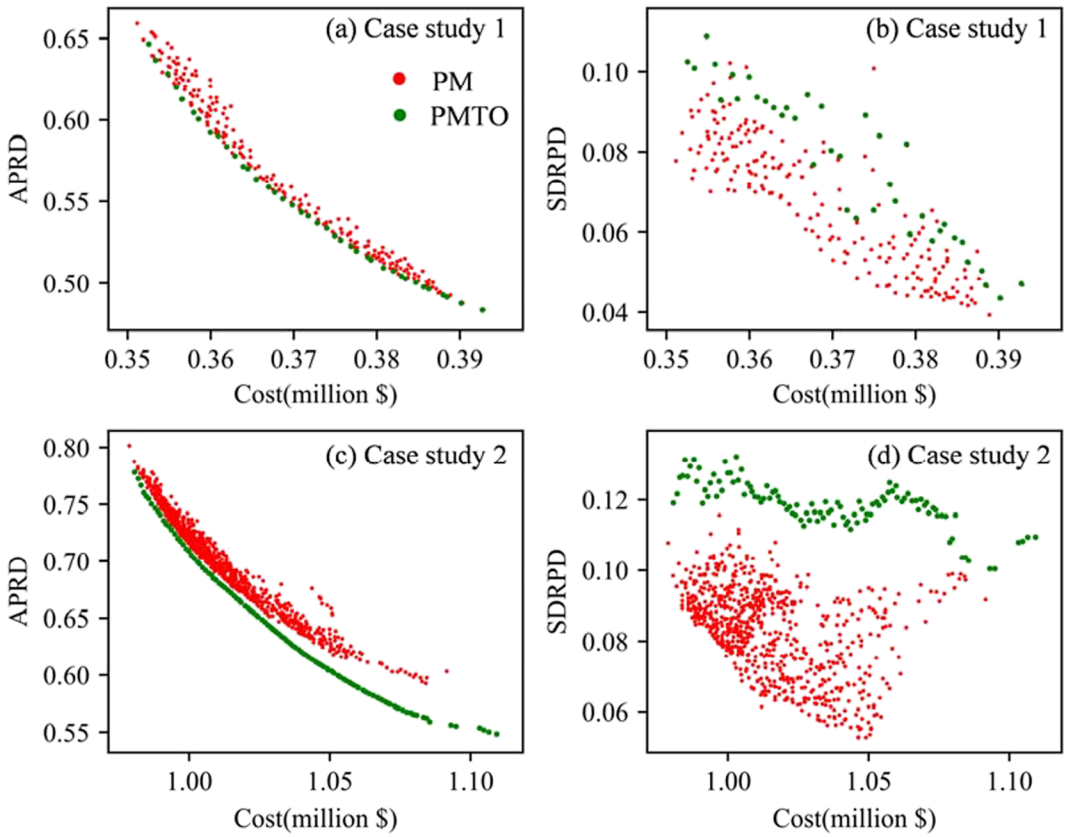

Figure 9. (a–d) Optimal fronts generated by the proposed PM with three objectives and the PMTO with two objectives.

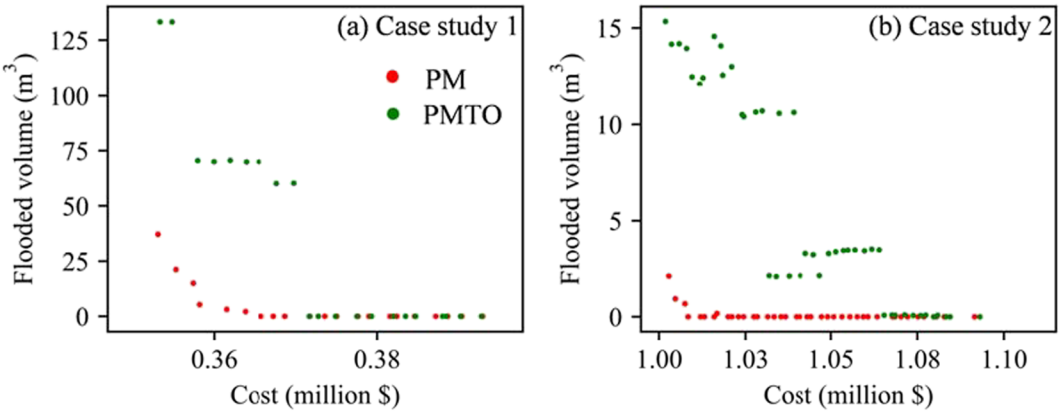

Figure 10. Flooded volumes of the selected solutions with similar cost for the (a, b) two case studies under an assumed rainfall event (20% increased intensity based on Figure 6).

APRD but significantly lower SDRPD values relative to the case when this objective is not included in the optimization. It is noted the number of PMTO solutions were appreciably lower than those from the PM with three objectives as shown in Figure 9. This is due to the use of adaptive population sizing strategy within the Borg algorithm (Hadka & Reed, 2013).

To verify the ability of the solutions in dealing with future uncertainties, the rainfall event in Figure 5 was assumed to increase 20% as a result of climate change (Zheng et al., 2015). To enable a fair comparison, a set of solutions with similar cost was selected from the fronts from the PM and PMTO. More specifically, a cost discretization with 2,000 dollars was defined, in which all the solutions from the PM and PMTO fronts within this discretization were considered to have a similar cost. This was followed by the hydraulic simulation for all these solutions using the assumed rainfall event (20% increased intensity based on Figure 5), and the solution from the PM and PMTO fronts with the lowest flooded volume was respectively selected to enable the comparison, with results presented in Figure 10.

It was seen from Figure 10 that the selected PM solutions had significantly lower flooded volumes compared to their corresponding PMTO solutions with similar costs. In addition, for the solutions with similar costs, the APRD values of the PM solutions were overall higher than those of the PMTO solutions as illustrated in Figures 9a and 9c. This indicated that lower flooded volumes of the selected PM solutions were attributed to their low values of SDRPD. This is because a solution with a lower APRD value could have some pipes with very high water levels (a high SDRPD value) under the given design storm, and manholes associated with these pipes were more likely to have overflows when the rainfall extremes increased in a changing climate. These results show that the inclusion of the objective of SDRPD within the multiobjective optimization framework can provide many solutions with great ability in handling future uncertainties, and hence, this objective is practically meaningful to facilitate the selection of appropriate design solutions for UDSs. In addition, the obtained PM and TOM results (Figure A1) showed that there existed a weak correlation between the SDRPD and APRD objectives for both case studies. This implied that while the SDRPD was a function of APRD within the calculation process, the SDRPD (estimated the variation of the water depth across the entire UDS) and the APRD (estimated the average water depth of the pipes within the UDS) measured the different properties of the design solutions. It was also noted that such a weak correlation between the APRD and SDRPD did not significantly affect the efficiency of the PM based on the analysis on the simulation results (Figure A2).

4.3. Efficiency Analysis of Different Optimization Methods

Figures 11 and 12 present the optimal fronts produced by the PM and the traditional method (TOM) applied to Case Study 1 and Case Study 2, respectively. This time 2-D plots are presented to enable better visualization. The numbers of evaluations in Figures 11a and 11b and Figures 12a and 12b were the minimum evaluations with which the nondominated feasible solutions were found by the TOM. Interestingly, approximate solutions identified by the proposed EBDM had overall similar front coverage with those of

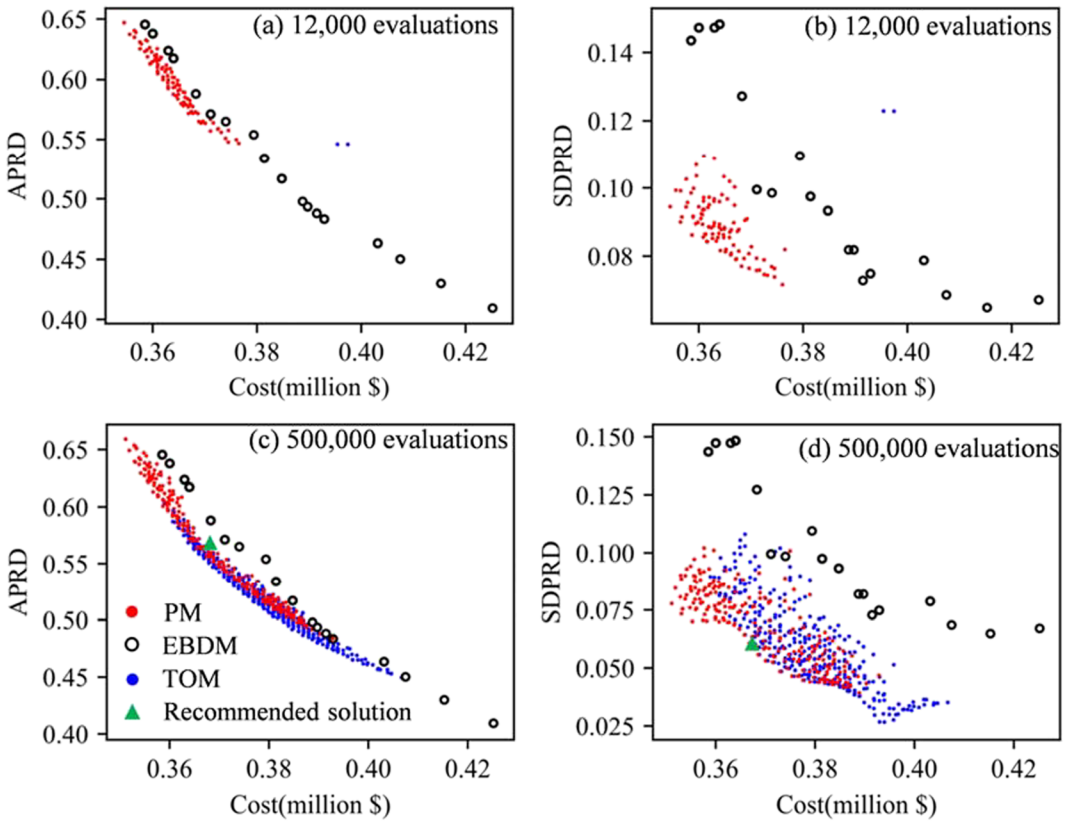

Figure 11. (a–d) Optimal fronts generated by the two different optimization methods applied to Case Study 1.

the final optimal fronts identified by the two optimization methods (Figures 11c and 11d and Figures 12c and 12d). In addition, these approximately solutions were reasonably close to the final fronts for both case studies. This further demonstrated the great effectiveness of the initial solutions produced by the proposed EBDM. Clearly, compared with the TOM which was initialized by purely random solutions, the PM initialized with approximate solutions exhibited significantly improved performance in identifying optimal fronts. Such an advantage has been consistently observed for repeated trials and was more prominent for the larger case study as shown in Figure 12. In this study, the PM has also been performed without the EBDM initial solutions for both case studies, and it was found that the quality of the obtained optimal fronts was significantly reduced. This further demonstrated that the advantage of the PM was caused by the use of the EBDM initial solutions within its optimization framework and the inclusion of Constraint 8 was used to ensure the practicality of the final solutions.

The running time for Case Study 1 with 12,000 evaluations and 500,000 evaluations was 15.6 and 66.5 hr, respectively, on a 2.9-GHz Dell PC (Inter R), and the running time for Case Study 2 with 98,000 evaluations and 500,000 evaluations was 35.1 and 180.4 hr, respectively, using the same computer configuration. The computational overheads used for the proposed EBDM was negligible (in the order of minutes) compared to those used in the optimization process.

Focusing on Case Study 1, only two feasible solutions were identified from the TOM after 12,000 Borg iterations (Figures 11a and 11b), but the PM was able to find 95 nondominated feasible solutions with substantially improved front coverage using the same computational overheads (15.6 running hours). In addition, the SDRPD values of these solutions were significantly lower than those offered by the TOM as illustrated in Figure 11b. For Case Study 2, there were only around 30 nondominated solutions found by the TOM using 98,000 evaluations (Figures 12a and 12b). However, the number of optimal solutions substantially increased when the PM was used (491 solutions) with the same running time (35.1 hr). More importantly, the optimal fronts yielded by the PM were substantially better than the TOM in both front coverage and quality. This

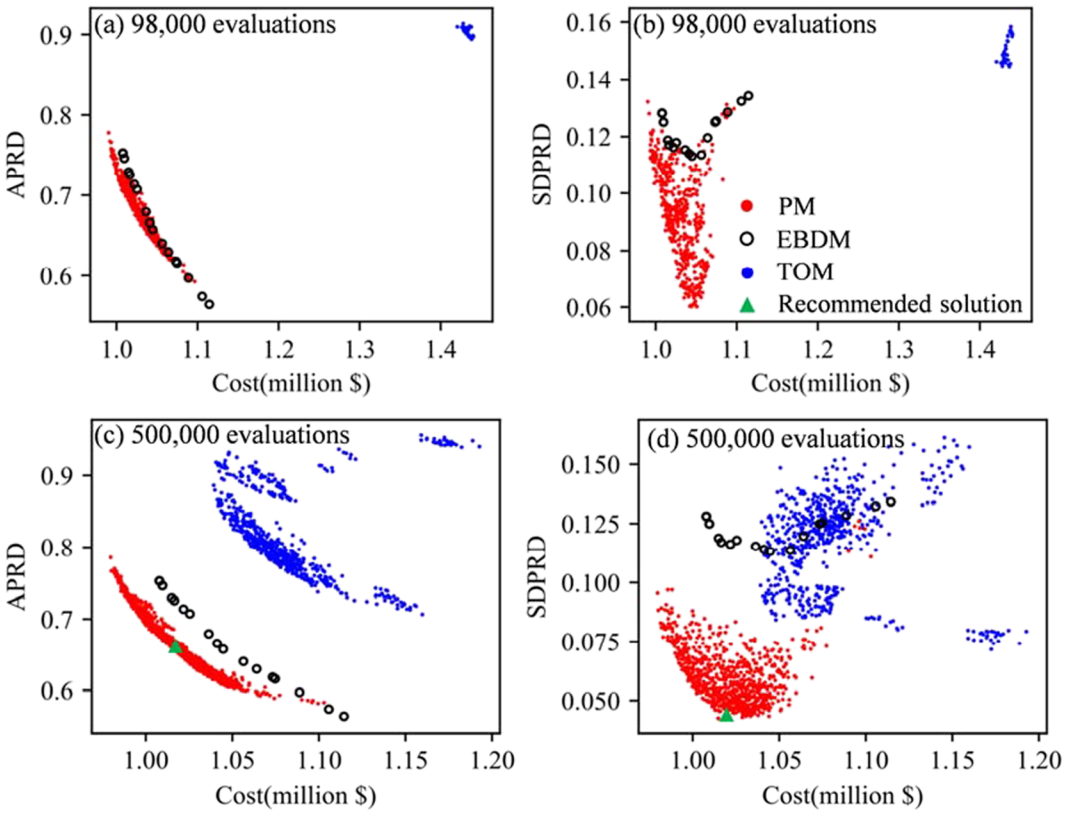

Figure 12. (a–d) Final optimal fronts produced by the two different optimization methods applied to Case Study 2.

implies that the PM was able to identify significantly improved fronts relative to the TOM with a relatively small number of evaluations allowed. This makes the PM particularly attractive for practical applications because the available computational budgets are often limited, especially for large and real-world UDS design problems.

When a larger number of evaluations were allowed (i.e., 500,000 evaluations), the optimal fronts of Case Study 1 produced by the PM were comparable to those offered by the TOM (Figures 11c and 11d), but this is not the case for Case Study 2. As shown in Figures 12c and 12d, the final optimal fronts yielded by the PM significantly outperformed those generated by the TOM. This implied that the advantage of the PM relative to the TOM was more prominent when dealing with large and complex real-word UDS design problems.

For each case study, a solution was recommended based on the final optimal front as shown in Figures 11 and 12, where the trade-off of the three objectives was considered. More specifically, a solution with the cost of 0.37 million dollars, APRD = 0.57 and SDRPD = 0.06 was selected for Case Study 1, and a solution with the cost of 1.03 million dollars, APRD = 0.65 and SDRPD = 0.04 was recommended for Case Study 2. The rationales behind these selections include (i) a solution with a relatively low SDRPD was desirable as it possessed a good ability in dealing with rainfall spatial variability in a changing climate, which was especially the case for relatively large catchments (e.g., the SDRPD was very low for the recommended solution of large Case Study 2), and (ii) a solution with the APRD between 0.5 and 0.8 was preferable as it would have better ability in handling the rainfall extremes due to climate change (Zheng et al., 2015) with reasonable cost. It was noted that the solutions with very low SDRPD values and high APRD values (e.g., a massive number of surcharged pipes) should be avoided during the decision-making process as they had a rather low reliability in dealing with rainfall and catchment uncertainties in future.

4.4. Solution Practicality Analysis of Different Optimization Methods

It should be highlighted again that the TOM results in Figures 11 and 12 did not consider the engineering criteria constraint (Equation 8) where the size of the pipe should be no smaller than the maximum

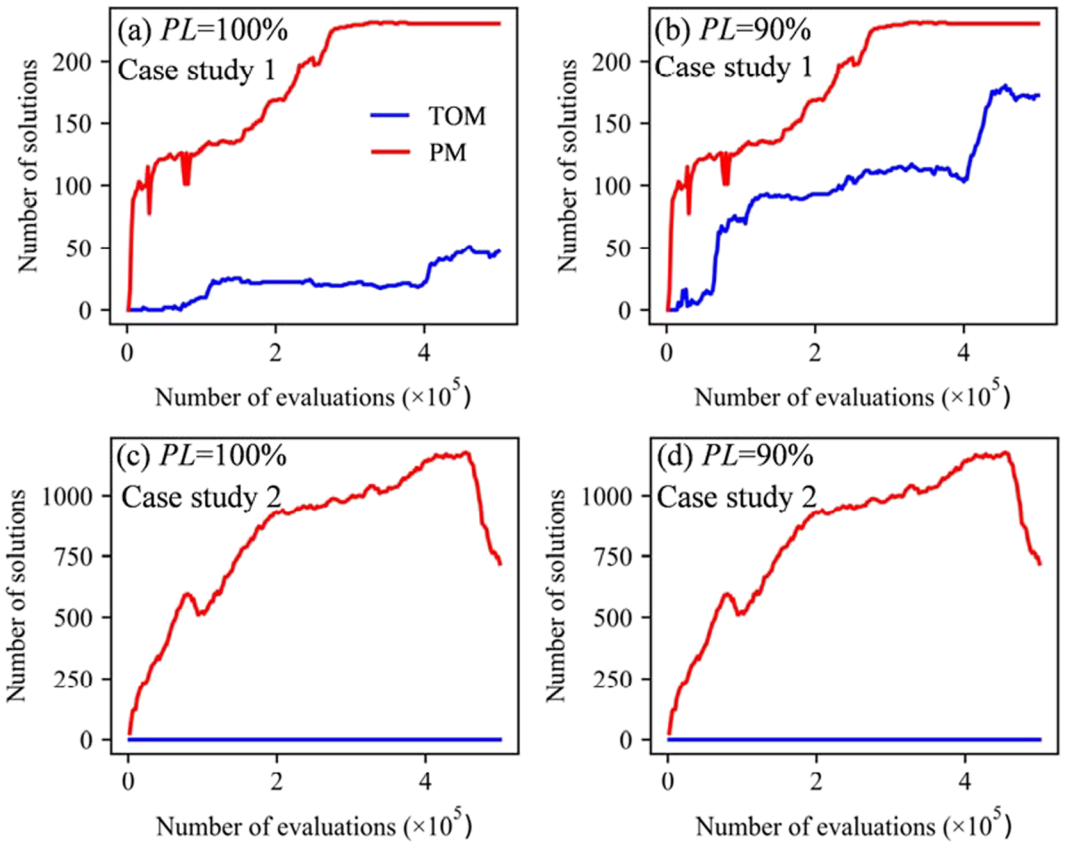

Figure 13. The values of *PL* of the two optimization methods applied to the (a–d) two case studies.

diameter of its corresponding upstream pipes. In this section, the optimal results of the TOM were assessed using the metric of the *PL* defined in Equations 17 and 18, with results given in Figure 13. As can be seen from this figure, the PM with the constraint of Equation 8 explicitly considered exhibited significantly better performance than the TOM in efficiently identifying optimal solutions with different *PL* values. For example, when $PL = 100\%$ was considered, a total number of 230 and 720 solutions was identified by the PM applied to Case Studies 1 and 2, respectively. However, these values were quite low for the TOM applied to Case Study 1 (43 solutions) and even 0 for large Case Study 2 (Figure 13d). When $PL = 90\%$ (the practicality constraint was partly released) was considered, the number of partly feasible solutions increased to 158 for the small Case Study 1, but still no solutions were found for the large Case Study 2 as shown in Figures 13b and 13d. This shows the merit in explicitly accounting for the engineering criterion within the optimization framework to ensure the practicality of the optimal solutions. It is noted that the number of nondominated solutions for Case Study 2 declined in the later searching stage, and this was caused by the use of adaptive population sizing and solution archive updating strategies within the Borg algorithm (Hadka & Reed, 2013).

5. Conclusions

This paper proposed a new multiobjective optimization method to design the UDSs, primarily aimed to improve the optimization efficiency and the practicality of the optimal solutions. The goal of the efficiency enhancement was achieved through the combination of a proposed EBDM and an MOEA approach. The EBDM was employed to identify a series of approximate solutions, which was subsequently used to initialize the MOEA search to improve the optimization efficiency. The goal of practicality improvement was attained by the inclusion of the optimization objective that accounted for the distribution properties of the peak relative water depths in pipes, as well as the inclusion of a practicality constraint to ensure sizes of downstream

pipes were no smaller than their corresponding upstream pipes. The PM was applied to two real-world UDS design problems of different scales, and Borg was used as the MOEA to enable optimization.

To enable a comprehensive comparison, the TOM with random initialization and without the consideration of the practicality constraint (Equation 8) was also applied to the two case studies. The key findings and implications are outlined below.

i While the solutions produced by the proposed EBDM were unable to entirely satisfy the design constraint (e.g., no flooding) when the true precipitation process curves were considered, they have been shown to be approximate optimal solutions as they were close to the final optimal fronts identified by the optimization algorithms (Figures 11 and 12).
ii It was demonstrated that the minimization of the standard deviation of relative peak water depths (SDRPD) in pipes (the proposed new objective) can effectively identify many solutions with great ability in dealing with future uncertainties (e.g., rainfall variations in a changing climate). Therefore, this objective can be an important supplement to the traditional objectives of cost and averaged relative peak water depths (ARPD), thereby facilitating the selection of appropriate design solutions for UDSs.
iii The PM initialized by the approximate solutions from the proposed EBDM was significantly more efficient than the TOM in identifying optimal fronts, and this advantage became more prominent for the larger case study (see Figures 11 and 12). In addition to the improved efficiency, the quality and coverage of the fronts produced by the PM were also substantially better than those generated by the TOM.
iv It was found that the majority of the solutions produced by the TOM were practically unacceptable as there were many pipes with diameters lower than their corresponding upstream pipes as shown in Figure 13. This highlighted the importance/necessity to explicitly account for the practicality constraint as implemented in the PM.

This study offers an efficient tool to optimally design real-world UDSs. This is significant for practical applications as in recent years urban floods have been increasingly occurring in many countries. It should be noted that the uncertainty associated with rainfall events (e.g., spatial variability) is not explicitly considered in the current method, and hence, an important future focus along this research line is to extend the proposed methodology to account for the uncertainty within the design process.

Data Availability Statement

All data/models used in this study have been submitted as the supporting documents.

Acknowledgments

This work is funded by the National Natural Science Foundation of China (Grant 51922096), Excellent Youth Natural Science Foundation of Zhejiang Province, China (LR19E080003), and Funds for International Cooperation and Exchange of the National Natural Science Foundation of China (51761145022). We also would like to appreciate the comments made by Tom Walski in improving the quality of this paper.

References

Ahmadi, A., Zolfagharipoor, M. A., & Nafisi, M. J. J. (2018). Development of a hybrid algorithm for the optimal design of sewer networks. *Journal of Water Resources Planning and Management*, *144*(8).

Arnbjerg-Nielsen, K. (2012). Quantification of climate change effects on extreme precipitation used for high resolution hydrologic design. *Urban Water Journal*, *9*(2), 57–65. https://doi.org/10.1080/1573062X.2011.630091

Barreto, W., Vojinovic, Z., Price, R., & Solomatine, D. (2010). Multiobjective evolutionary approach to rehabilitation of urban drainage systems. *Journal of Water Resources Planning and Management-Asce*, *136*(5), 547–554.

Beijing General Municipal Engineering Design, & Research Institute (2017). *Water supply and drainage handbook: Urban drainage*, (p. 20). Beijing, China: China Architecture & Building Press.

Berg, P., Moseley, C., & Haerter, J. O. (2013). Strong increase in convective precipitation in response to higher temperatures. *Nature Geoscience*, *6*(3), 181–185. https://doi.org/10.1038/ngeo1731, https://www.nature.com/articles/ngeo1731#supplementary-information

Broad, D. R., G. C. Dandy, and H. R. Maie (2004). "A metamodeling approach to water distribution system optimization." *Critical Transitions in Water and Environmental Resources Management*, Salt Lake City, UT.

Butler, D., James Digman, C., Makropoulos, C., & Davies, J. (2018). *Urban drainage*. Boca Raton, FL: CRC Press. https://doi.org/10.1201/9781351174305

CDOWE (Code for Design of Outdoor Wastewater Engineering) (2014). Design manual for outdoor wastewater engineering. The People's Republic of China Ministry of Housing and Urban Rural Development: 12–28

Dawadi, S., & Ahmad, S. (2012). Changing climatic conditions in the Colorado River basin: Implications for water resources management. *Journal of Hydrology*, *430*, 127–141.

Duan, H. F., Li, F., & Tao, T. (2016). Multi-objective optimal design of detention tanks in the urban stormwater drainage system: Uncertainty and sensitivity analysis. *Water Resources Management*, *30*(7), 2213–2226. https://doi.org/10.1007/s11269-016-1282-1

Duan, H. F., Li, F., & Yan, H. X. (2016). Multi-objective optimal design of detention tanks in the urban stormwater drainage system: LID implementation and analysis. *Water Resources Management*, *30*(13), 4635–4648. https://doi.org/10.1007/s11269-016-1444-1

Farmani, R., Walters, G. A., & Savic, D. A. (2005). Trade-off between total cost and reliability for Anytown water distribution network. *Journal of Water Resources Planning and Management-Asce*, *131*(3), 161–171. https://doi.org/10.1061/(ASCE)0733-9496(2005)131:3(161)

Fu, G., & Butler, D. (2014). Copula-based frequency analysis of overflow and flooding in urban drainage systems. *Journal of Hydrology*, *510*, 49–58. https://doi.org/10.1016/j.jhydrol.2013.12.006

Fu, G., Khu, S. T., & Butler, D. (2009). Use of surrogate modelling for multiobjective optimisation of urban wastewater systems. *Water Science and Technology*, *60*(6), 1641–1647. https://doi.org/10.2166/wst.2009.508
Gulbaz, S., & Kazezyilmaz-Alhan, C. M. (2017). Experimental investigation on hydrologic performance of LID with rainfall-watershed-bioretention system. *Journal of Hydrologic Engineering*, *22*(1), D4016003.
Gupta, R. S. (2016). *Hydrology and hydraulic systems*, Illinois, USA: Waveland Press.
Hadka, D., & Reed, P. (2013). Borg: An auto-adaptive many-objective evolutionary computing framework. *Evolutionary Computation*, *21*(2), 231–259. https://doi.org/10.1162/EVCO_a_00075
Hammond, M. J., Chen, A. S., Butler, D., Djordjevic, S., & Manojlovic, N. (2013). A framework for flood impact assessment in urban areas. In A. Chavoshian & K. Takeuchi (Eds.), *Floods: From risk to opportunity* (p. 41).
Hassan, W. H., Jassem, M. H., & Mohammed, S. S. (2018). A GA-HP model for the optimal design of sewer networks. *Water Resources Management*, *32*(3), 865–879. https://doi.org/10.1007/s11269-017-1843-y
Hoss, F., Fischbach, J., & Molina-Perez, E. (2016). Effectiveness of best management practices for Stormwater treatment as a function of runoff volume. *Journal of Water Resources Planning and Management*.
Houng, H. T. L., & Pathirana, A. (2013). Urbanization and climate change impacts on future urban flooding in Can Tho city, Vietnam. *Hydrology and Earth System Sciences*, *17*(1), 379–394. https://doi.org/10.5194/hess-17-379-2013
Jato-Espino, D., Sillanpaa, N., Charlesworth, S. M., & Andres-Domenech, I. (2016). Coupling GIS with stormwater modelling for the location prioritization and hydrological simulation of permeable pavements in urban catchments. *Water*, *8*(10), 451. https://doi.org/10.3390/w8100451
Li, F., Duan, H. F., Yan, H. X., & Tao, T. (2015). Multi-objective optimal design of detention tanks in the urban stormwater drainage system: Framework development and case study. *Water Resources Management*, *29*(7), 2125–2137. https://doi.org/10.1007/s11269-015-0931-0
Liu, H., Zhang, C., Jiang, Y., Meng, F., & Fu, G. (2018). Measuring surplus capacity for multiobjective optimal design of foul sewer systems. *Urban Water Journal*, *15*(8), 723–731. https://doi.org/10.1080/1573062x.2018.1561907
Lowe, S. A. (2010). Sanitary sewer design using EPA storm water management model (SWMM). *Computer Applications in Engineering Education*, *18*(2), 203–212.
Maier, H. R., Kapelan, Z., Kasprzyk, J., Kollat, J., Matott, L. S., Cunha, M. C., et al. (2014). Evolutionary algorithms and other metaheuristics in water resources: Current status, research challenges and future directions. *Environmental Modelling & Software*, *62*, 271–299. https://doi.org/10.1016/j.envsoft.2014.09.013
Mccuen, R. H. (2004). Hydrologic analysis and design. *Journal of the American Water Resources Association*, *40*(3), 838.
Mohammadiun, S., Yazdi, J., Neyshabouri, S. A. A. S., & Sadiq, R. (2018). Development of a stochastic framework to design/rehabilitate urban stormwater drainage systems based on a resilient approach. *Urban Water Journal*, *15*(2), 167–176. https://doi.org/10.1080/1573062x.2018.1424218
Navarro, I. (2009). In *Optimized network of urban drainage design (Master thesis)* (p. 1–10). Bogotá, Colombia: Universidad de los Andes.
Navin, P. K., Mathur, Y. P., & Kumar, D. (2019). Layout optimization of sewer network using minimum cumulative flow in the sewer network. In *Advances in waste management* (pp. 333–343). Singapore: Springer.
Ngamalieu-Nengoue, U. A., Javier Martinez-Solano, F., Iglesias-Rey, P. L., & Mora-Melia, D. (2019). Multi-objective optimization for urban drainage or sewer networks rehabilitation through pipes substitution and storage tanks installation. *Water*, *11*(5). https://doi.org/10.3390/w11050935
Pan, C. L., Wang, X. W., Liu, L., Huang, H. B., & Wang, D. S. (2017). Improvement to the huff curve for design storms and urban flooding simulations in Guangzhou, China. *Water*, *9*(6), 411. https://doi.org/10.3390/w9060411
Rossman L. A. (2010). *Storm water management model user's manual version 5.0 (EPA/600/R-05040)*. Washington, DC: US Environmental Protection Agency.
Schmitt, T. G., Thomas, M., & Ettrich, N. (2004). Analysis and modeling of flooding in urban drainage systems. *Journal of Hydrology*, *299*(3–4), 300–311. https://doi.org/10.1016/S0022-1694(04)00374-9
Vojinovic, Z., Sahlu, S., Torres, A. S., Seyoum, S. D., Anvarifar, F., Matungulu, H., & Kapelan, Z. (2014). Multi-objective rehabilitation of urban drainage systems under uncertainties. *Journal of Hydroinformatics*, *16*(5), 1044–1061. https://doi.org/10.2166/hydro.2014.223
Walski, T. M. (2001). The wrong paradigm—Why water distribution optimization doesn't work. *Journal of Water Resources Planning and Management*, *127*(4), 203–205. https://doi.org/10.1061/(ASCE)0733-9496(2001)127:4(203)
Wang, Q., Guidolin, M., Savic, D., & Kapelan, Z. (2015). Two-objective design of benchmark problems of a water distribution system via MOEAs: Towards the best-known approximation of the true Pareto front. *Journal of Water Resources Planning and Management*, *141*(3), 04014060. https://doi.org/10.1061/(ASCE)WR.1943-5452.0000460
Wang, Q., Zhou, Q., Lei, X., & Savic, D. (2018). Comparison of multiobjective optimization methods applied to urban drainage adaption problems. *Journal of Water Resources Planning and Management*, *144*(11), 04018070. https://doi.org/10.1061/(ASCE)WR.1943-5452.0000996
Wasko, C., & Sharma, A. (2015). Steeper temporal distribution of rain intensity at higher temperatures within Australian storms. *Nature Geoscience*, *8*(7), 527–529. https://doi.org/10.1038/ngeo2456
Westra, S., Fowler, H. J., Evans, J. P., Alexander, L. V., Berg, P., Johnson, F., & Roberts, N. M. (2014). Future changes to the intensity and frequency of short-duration extreme rainfall. *Reviews of Geophysics*, *52*, 522–555. https://doi.org/10.1002/2014RG000464
Yazdi, J. (2018). Rehabilitation of urban drainage systems using a resilience-based approach. *Water Resources Management*, *32*(2), 721–734. https://doi.org/10.1007/s11269-017-1835-y
Yen, B. C. (1992). Dimensionally homogeneous Manning's formula. *Journal of Hydraulic Engineering*, *118*(9), 1326–1332. https://doi.org/10.1061/(ASCE)0733-9429(1992)118:9(1326)
Yu, J., Qin, X., Chiew, Y. M., Min, R., & Shen, X. (2017). Stochastic optimization model for supporting urban drainage design under complexity. *Journal of Water Resources Planning and Management*, *143*(9), 05017008. https://doi.org/10.1061/(ASCE)WR.1943-5452.0000806
Zheng, F., Westra, S., & Leonard, M. (2015). Opposing local precipitation extremes. *Nature Climate Change*, *5*(5), 389–390. https://doi.org/10.1038/nclimate2579
Zheng, F., Westra, S., Leonard, M., & Sisson, S. A. (2014). Modeling dependence between extreme rainfall and storm surge to estimate coastal flooding risk. *Water Resources Research*, *50*, 2050–2071. https://doi.org/10.1002/2013WR014616
Zheng, F., Zecchin, A., Newman, J., Maier, H., & Dandy, G. (2017). An adaptive convergence-trajectory controlled ant colony optimization algorithm with application to water distribution system design problems. *IEEE Transactions on Evolutionary Computation*, *21*(5), 773–791. https://doi.org/10.1109/TEVC.2017.2682899

Zheng, F. F., Zecchin, A. C., Maier, H. R., & Simpson, A. R. (2016). Comparison of the searching behavior of NSGA-II, SAMODE, and Borg MOEAs applied to water distribution system design problems. *Journal of Water Resources Planning and Management*, *142*(7).

Zhou, Q. (2014). A review of sustainable urban drainage systems considering the climate change and urbanization impacts. *Water*, *6*(4), 976–992. https://doi.org/10.3390/w6040976